

Regulation strategies of hot carrier cooling process in perovskite nanocrystals

Zhenyao Tan(谭振耀), Kexin Xu(徐可欣), Yi Chen(陈逸), Can Ren(任璨), and Tingchao He(贺廷超)
Citatio: Chin. Phys. B, 2025, 34 (**9**): 097302. DOI: 10.1088/1674-1056/ade24d
http://cpb.iphy.ac.cn; http://iopscience.iop.org/cpb

What follows is a list of articles you may be interested in

Hot carrier cooling in lead halide perovskites probed by two-pulse photovoltage correlation spectroscopy

Yuqing Huang(黄玉清), Chaoyu Guo(郭钞宇), Lei Gao(高蕾), Wenna Du(杜文娜), Haotian Zheng(郑浩天), Da Wu(吴达), Zhengpu Zhao(赵正朴), Chu-Wei Zhang(张楚惟), Qin Wang(王钦), Xin-Feng Liu(刘新风), Qingfeng Yan(严清峰), and Ying Jiang(江颖)
Chin. Phys. B, 2024, 33 (**10**): 107304. DOI: 10.1088/1674-1056/ad7728

Nonlinear Seebeck and Peltier effects in a Majorana nanowire coupled to leads

Feng Chi(迟锋), Jia Liu(刘佳), Zhenguo Fu(付振国), Liming Liu(刘黎明), and Zichuan Yi(易子川)
Chin. Phys. B, 2024, 33 (**7**): 077301. DOI: 10.1088/1674-1056/ad3f99

Manipulation of internal blockage in triangular triple quantum dot

Yue Qi(齐月) and Jian-Hua Wei(魏建华)
Chin. Phys. B, 2024, 33 (**5**): 057301. DOI: 10.1088/1674-1056/ad2d54

Chiral current regulation and detection of Berry phase in triangular triple quantum dots

Yue Qi(齐月), Yi-Ming Liu(刘一铭), Yuan-Dong Wang(王援东), Jian-Hua Wei(魏建华), and Zhen-Gang Zhu(朱振刚)
Chin. Phys. B, 2023, 32 (**8**): 087304. DOI: 10.1088/1674-1056/acd36c

Coherent manipulation of a tunable hybrid qubit via microwave control

Si-Si Gu(顾思思), Bao-Chuan Wang(王保传), Hai-Ou Li(李海欧), Gang Cao(曹刚), and Guo-Ping Guo(郭国平)
Chin. Phys. B, 2023, 32 (**8**): 087302. DOI: 10.1088/1674-1056/acd0a7

TOPICAL REVIEW — Exciton physics: Fundamentals, materials and devices

Regulation strategies of hot carrier cooling process in perovskite nanocrystals

Zhenyao Tan(谭振耀)[1,†], Kexin Xu(徐可欣)[1,†], Yi Chen(陈逸)[1], Can Ren(任璨)[2,‡], and Tingchao He(贺廷超)[1,§]

[1] *Key Laboratory of Optoelectronic Devices and Systems of Ministry of Education and Guangdong Province, College of Physics and Optoelectronic Engineering, Shenzhen University, Shenzhen* 518060, *China*

[2] *School of Artificial Intelligence, Shenzhen Polytechnic University, Shenzhen* 518055, *China*

(Received 29 April 2025; revised manuscript received 6 June 2025; accepted manuscript online 9 June 2025)

Recent breakthroughs in hot carrier (HC) cooling dynamics within halide perovskite nanocrystals (NCs) have positioned them as promising candidates for next-generation optoelectronic applications. Therefore, it is of great importance to systematically summarize advances in understanding and controlling HC relaxation mechanisms. Here, we offer an overview of advances in the understanding of the HC cooling process in perovskite NCs, with a focus on influences of excitation energy, excitation intensity, composition, size, dimensionality, doping, and core–shell structure on the HC cooling times. Finally, we propose suggestions for future investigations into the HC cooling process in perovskite NCs.

Keywords: perovskite nanocrystals, hot carrier cooling, ultrafast dynamics

PACS: 73.21.La, 33.50.Dq, 63.20.kd, 78.67.Bf

DOI: 10.1088/1674-1056/ade24d **CSTR:** 32038.14.CPB.ade24d

1. Introduction

In recent years, perovskite nanocrystals (NCs) have been used extensively in optoelectronic devices such as light-emitting diodes (LEDs),[1,2] lasers,[3–5] solar cells, and nonlinear optics,[6] due to their wide luminescence wavelength tunability and exceptional photothermal stability.[7,8] The hot carrier (HC) cooling process can significantly impact the overall performance of these devices. For example, fast HC cooling rates are advantageous for certain emission-related applications, particularly in lasers and LEDs.[9,10] Furthermore, the cooling time of HC directly influences the potential of high-speed optoelectronic devices in key performance indicators such as cutoff frequency.[11] When the cooling time is shortened to approximately 0.3 ps or less, the switching time of optoelectronic devices (such as photodetectors and all-optical switches) can reach the terahertz frequency band.[12] However, in solar cells, rapid HC cooling significantly accelerates non-adiabatic recombination, leading to greater energy loss,[13,14] which is the primary reason that prevents single-junction solar cells from surpassing the Shockley–Queisser limit.[15] To enhance efficiency, some researchers have attempted to extract HCs during the cooling process.[16–19] However, current studies indicate that reusing the heat generated during this process remains challenging.[20,21] Therefore, a more feasible way to minimize energy loss is to modulate the HC cooling process.[18] To optimize the performance of perovskite NCs in optoelectronic devices, it is crucial to understand the HC cooling process and explore regulation strategies.[12]

Recent breakthroughs in the study of HC cooling processes in perovskite NCs have marked significant progress.[22–24] Given these advancements, a comprehensive review of the HC cooling mechanisms in perovskite NCs is both timely and essential. This review provides a detailed summary of the factors influencing the HC cooling process, including excitation energy, excitation intensity, composition, size, dimensionality, doping, and core–shell structure. Finally, we discuss prospective opportunities and challenges in advancing research on HC cooling in perovskite NCs.

2. Basic description of the HC cooling process

Charge carriers with excess energy above the band gap produced by absorbing photons are known as HCs, which have temperatures higher than the lattice temperature.[25–28] These HCs first release excess energy mainly through electron-phonon (EP) coupling; then longitudinal optical (LO) phonons decay into acoustic phonons, which subsequently diffuse the energy into the lattice. The HCs rapidly relax to the energy band edge on sub-picosecond time scales, a process known as HC cooling.[26,29,30]

The HC cooling process can be affected by multiple factors, many of which often occur simultaneously, such as excitation energy, EP coupling strength, defect density, phonon density, quantum confinement effects, and large polaron formation.[31,32] Among them, EP coupling is the main

[†]These authors contributed equally to this work.

[‡]Corresponding author. E-mail: rencan@szpu.edu.cn

[§]Corresponding author. E-mail: tche@szu.edu.cn

© 2025 Chinese Physical Society and IOP Publishing Ltd. All rights, including for text and data mining, AI training, and similar technologies, are reserved.

pathway for HC cooling in perovskites. Strong EP interactions couple to lattice distortions, which are responsible for large polaron formation.[33] In addition, the effect of HC density on its cooling kinetics is very significant. Different carrier densities induce different cooling mechanisms. At lower carrier density, the HC cooling process exhibits intrinsic material properties. At relatively high carrier density, other physical phenomena also arise, such as the hot phonon bottleneck (HPB) effect[34–36] ($\approx 10^{18}$ cm^{-3}), Auger heating[33,34,37] ($\approx 10^{19}$ cm^{-3}), and the state-filling effect[38] ($\approx 10^{19}$ cm^{-3}). All these mechanisms significantly affect the HC cooling process.

In the following, we analyze the effects of these factors on the HC cooling process, starting from excitation energy, excitation intensity, composition, size, dimensionality, doping, and epitaxial shell layer. Due to space limitations, only representative studies are discussed regarding the HC cooling process.

3. HC cooling in perovskite NCs

3.1. Impact of excitation energy

The excitation energy affects the excess energy of the HCs, and larger excess energy generally leads to longer HC cooling times.[19,39] Niu *et al.*[30] showed that, in both undoped and Ni^{2+}-doped $CsPbI_3$ NCs, increasing excitation energy prolonged HC cooling times. Similarly, Shukla *et al.*[40] observed slower HC cooling in $CsPbBr_3$ NCs when excited at 300 nm compared to 420 nm. Li *et al.*[41] found that the HC cooling time of $FAPbI_3$ (FA, formamidinium, $CH(NH_2)_2^+$) NCs (7.5 nm) increases with increasing excitation energy for excitations below two bandgap energies ($2E_g$). However, at excitation energies above the multiple exciton generation threshold (MEG_{th}), HC cooling instead becomes faster (Figs. 1(a) and 1(b)). This is attributed to the fact that MEG occurs through the anti-Auger process, and the multiexciton shares the excess energy after excitation. Moreover, Meng *et al.*[42] found that at low excitation energies (near-bandgap excitation), HCs of Mn-doped $CsPbI_3$ NCs are unable to accelerate relaxation via the Mn orbital pathway. Instead, Mn doping widens the phonon band gap and slows down HC cooling. At high excitation energies, the Mn orbital pathway dominates and accelerates HC cooling (Figs. 1(c) and 1(d)).

3.2. Impact of excitation density

Carrier density significantly affects the HC cooling process, and high carrier density generally induces the HPB effect, mainly generated by the suppression of the Klemens channel for LO phonon decay. Fu *et al.*[34] found that at a carrier density of 10^{18} cm^{-3}, the emergence of the HPB effect led to slow HC cooling. When carrier density exceeds 10^{19} cm^{-3}, the HPB in $MAPbI_3$ (MA, methylammonium, $CH_3NH_3^+$) and the Auger heating effect together further hinder HC cooling (Fig. 2(a)). Li *et al.*[19] found in $MAPbBr_3$ NCs that Auger heating slowed down HC cooling at high carrier density. Zhang *et al.*[43] also concluded that HCs in $MAPbBr_3$ NCs cool slowly at high excitation intensities. Dai *et al.*[24] found that in $MASnI_3$ NCs, when the initial carrier density was below 10^{18} cm^{-3}, HCs cooled rapidly mainly through Fröhlich interactions. When the injected carrier density exceeds $\sim 10^{18}$ cm^{-3}, the HC cooling rate decreases due to the HPB and non-radiative Auger heating processes, and the average carrier cooling time of $MASnI_3$ NCs is prolonged by ~ 7 ps. Papagiorgis *et al.*[44] found that both effects are also present in $FAPbI_3$ NCs at high excitation intensities, slowing down HC cooling. Similarly, Hopper *et al.*[45] observed the HPB effect in $CsPbBr_3$ NCs at high excitation intensities. This shows that excitation intensity has a significant effect on many materials. Moreover, the intrinsic properties of the material are weakened at high excitation intensity. For example, Meng *et al.*[42] found that in Mn-doped $CsPbI_3$ NCs, the phonon bandgap widening due to Mn doping originally dominated at low excitation energies. However, at high excitation intensities, the relaxation paths introduced by Mn doping are also involved due to the Moss–Burstein effect, making it difficult to distinguish from HC dynamics in undoped NCs.

Appropriate conditions can suppress the HPB and Auger heating effects. Cong *et al.*[39] found that strong quantum confinement due to the small size in $CsPbI_3$ NCs suppresses the HPB effect. Niu *et al.*[30] investigated HC cooling in Ni-doped $CsPbI_3$ NCs and found that while high carrier density ($\langle N_0 \rangle = 20$) induces HPB and Auger heating, Ni doping can inhibit them to some extent, thus accelerating HC cooling (Fig. 2(b)). Ye *et al.*[46] investigated HC cooling in $CsPbBr_3$ and $CsPbBr_xI_{3-x}$ NCs with different defect densities. They found that for NCs with low defect densities, high carrier densities lead to HPB and Auger heating, which slow down HC cooling. However, for NCs with medium or high defect densities, these two effects are attenuated, thereby accelerating HC cooling (Figs. 2(c) and 2(d)). Additionally, Dai *et al.*[47] reported anomalously fast cooling of $FASnI_3$ NCs at high carrier density, due to the predominance of the multiple exciton effect, providing a new pathway for HC relaxation.

3.3. Impact of components

Differences in NC composition directly influence intrinsic optical properties, including HC cooling rates. Focusing on the A-site cations of perovskite, Yang *et al.*[48] observed that the carrier-phonon relaxation rate of $FAPbI_3$ is roughly an order of magnitude slower than in cesium-based counterparts. They attributed this difference to the introduction of organic cations, which promote upconversion of acoustic to optical phonons, effectively slowing the cooling process via reheating.[49] Moreover, Chan *et al.*[15] concluded that organic-based perovskites (MA, FA) cool more slowly than inorganic $CsPbBr_3$. This slower rate can be attributed to the faster formation of large polarons in the hybrid system,[50] which effectively screens the Coulombic interaction between carriers and LO phonons,[51,52] thus slowing HC cooling.

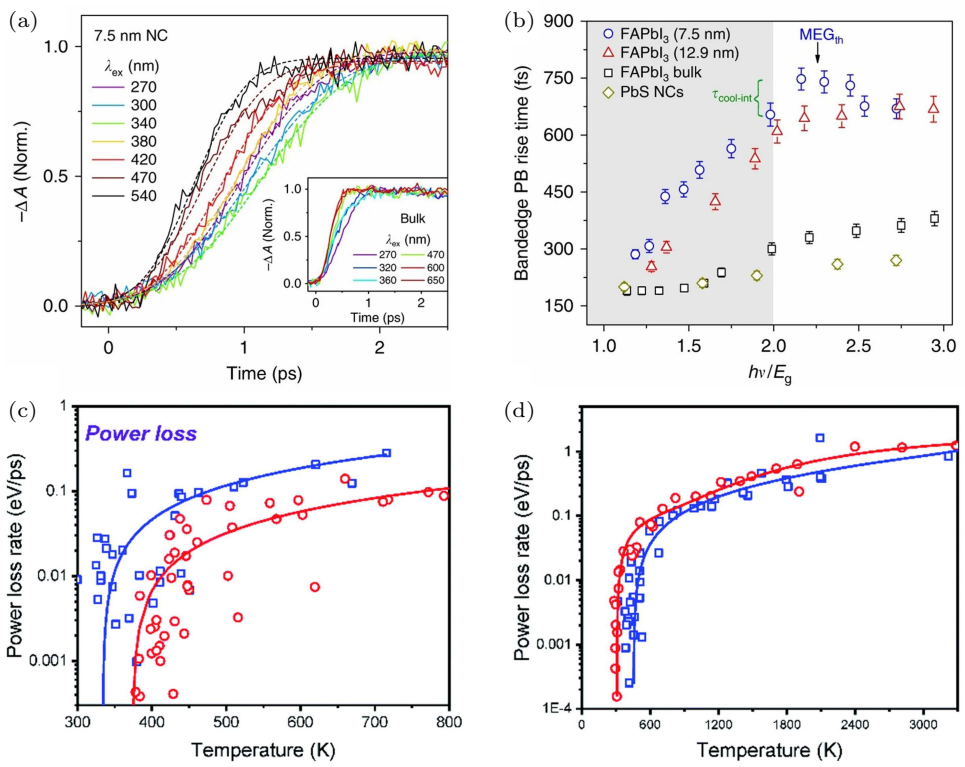


Fig. 1. (a) Normalized band-edge photobleaching dynamics of 7.5 nm $FAPbI_3$ NCs at different excitation wavelengths. The dashed line represents a single-exponential fit. The inset illustrates the bulk material case.[41] (b) Band-edge photobleaching rise times of perovskite and PbS NCs at different excitation energies. The gray area indicates the MEG threshold with energies below $2E_g$.[41] (c) Power loss of Mn-doped $CsPbI_3$ NCs at carrier temperatures excited at 570 nm, and (d) at 400 nm. The blue and red lines represent $CsPbI_3$ and Mn-doped $CsPbI_3$ NCs, respectively.[42]

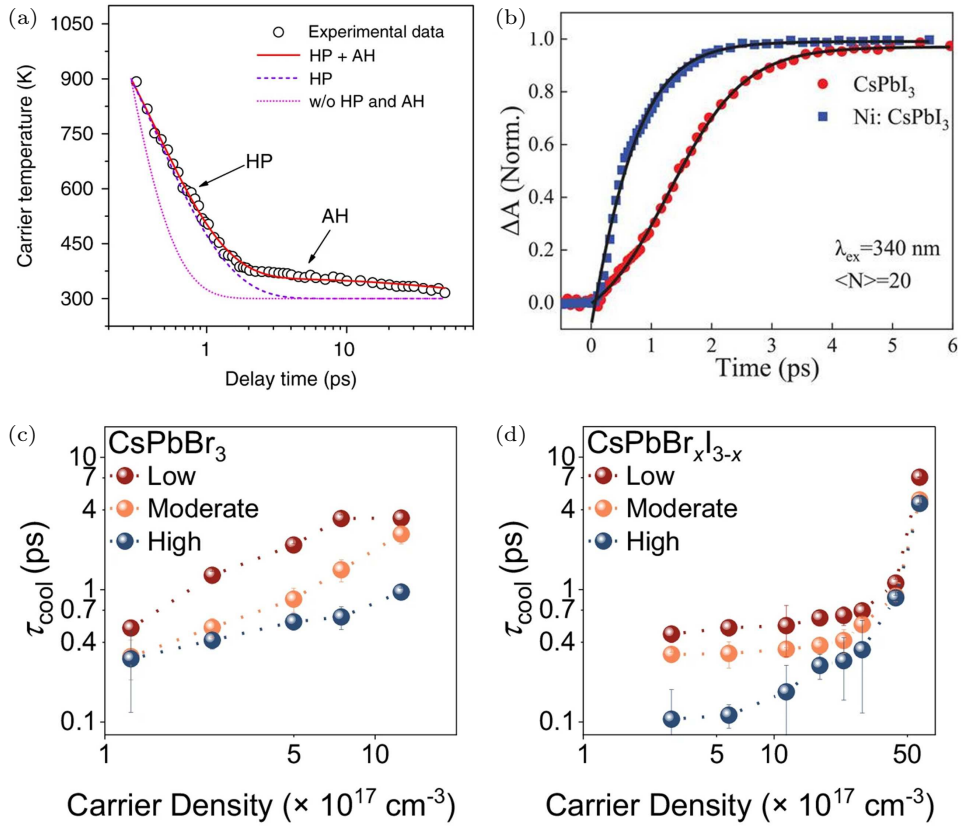


Fig. 2. (a) Temperature variation of HCs in $MAPbI_3$ under 2.48 eV excitation, with a carrier density of 0.4×10^{18} cm^{-3}. The red line shows the fit including both hot phonon and Auger heating effects, the purple line shows only the hot phonon effect, and the magenta line shows neither hot phonon nor Auger heating effects.[34] (b) TA signal rise times of $CsPbI_3$ and Ni:$CsPbI_3$ NCs probed at the band edge under 340 nm excitation.[30] HC cooling times of (c) $CsPbBr_3$ NCs and (d) $CsPbBr_xI_{3-x}$ NCs at different defect and carrier densities.[46]

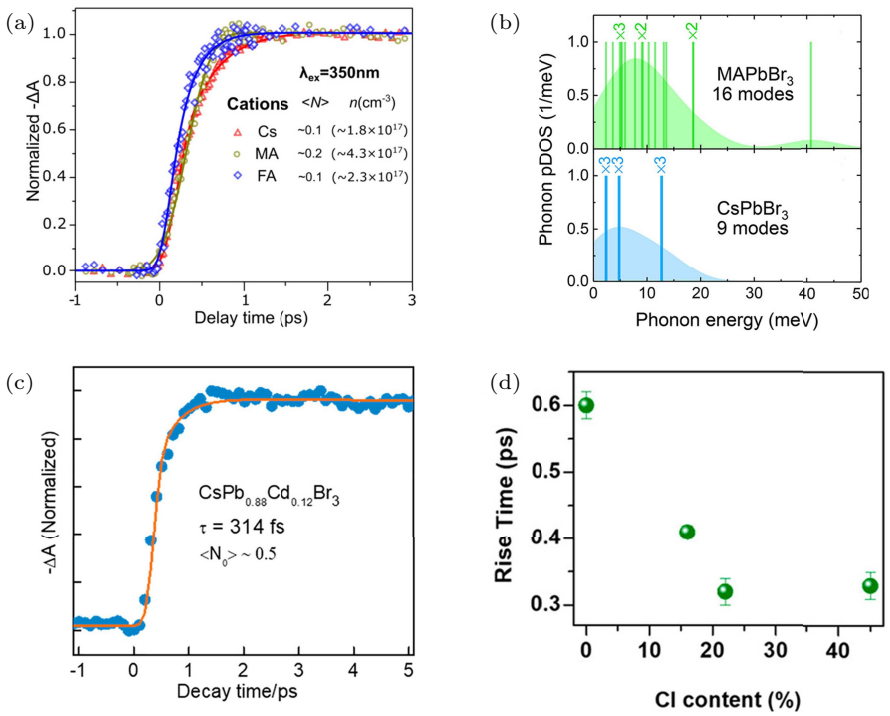


Fig. 3. (a) Bleaching dynamics of $CsPbBr_3$, $MAPbBr_3$, and $FAPbBr_3$ NCs.[27] (b) Schematic diagrams of calculated phonon modes in $MAPbBr_3$ and $CsPbBr_3$. Doubly (×2) and triply (×3) degenerate modes are indicated.[57] (c) Rise time of ground-state bleaching signal of $CsPb_{0.88}Cd_{0.12}Br_3$ NCs excited at 350 nm.[60] (d) Rise time of photobleaching signal for $CsPbBr_3$ with varying Cl content.[64]

However, the HC cooling rate in perovskite NCs shows an opposite trend. Chen *et al.*[27] reported that, at low excitation intensities and identical excitation energies, the HC cooling times of $APbBr_3$ (A = MA, FA, Cs) NCs follow the order $CsPbBr_3$ > $MAPbBr_3$ > $FAPbBr_3$ (Fig. 3(a)). This can be attributed to two mechanisms. On one hand, the organic A-site cations (MA and FA) interact more strongly with the Pb–Br frameworks due to their larger size compared to Cs, thereby enhancing EP coupling. In contrast, the smaller Cs cations exhibit limited mobility.[22,27,53–56] On the other hand, the presence of MA and FA cations introduces additional phonon modes,[54,55] which contribute to an increase in the phonon density of states (DOS),[27,57] as illustrated in Fig. 3(b). A similar study conducted by our group showed that the introduction of organic A-site cations (R-1-(1-naphthyl)ethylammonium, R-NEA) resulted in films with faster HC cooling rates, supporting the above viewpoint by enhanced EP coupling.[58] In addition, under similar conditions, MA-based NCs exhibit a weaker Auger heating effect compared to Cs-based NCs, which also helps explain the faster HC cooling in organic-cation-based perovskites.[59] Overall, the effect of A-site cations on HC cooling is not yet fully understood, and further studies are needed to establish a comprehensive explanation.[53]

Modulation of the B-site elements can also affect HC cooling behavior. Dai *et al.*[47] found that Sn-based $FASnI_3$ NCs exhibit stronger quantum confinement, leading to the separation of energy levels. As a result, even at low carrier density, $FASnI_3$ NCs show HC cooling times 50–100 times longer than those of Pb-based NCs under the same excitation conditions. Building on this, Dai *et al.*[24] further demonstrated that increasing Sn content in Pb–Sn alloy perovskite NC systems can effectively slow down HC cooling. In contrast, our group's investigation of $CsPb_xCd_{1-x}Br_3$ ($x = 1$, 0.93, 0.88) NCs revealed that Cd-alloyed NCs exhibit shorter cooling times (Fig. 3(c)).[60] Similar conclusions were drawn for $CsPb_{0.8}Zn_{0.2}I_3$ NCs.[61] Thus, the effect of alloying on HC relaxation should be analyzed in the context of specific conditions.

Previous literature has shown that X-site elements can also significantly affect HC cooling in perovskite NCs.[21,62,63] Soetan and coworkers investigated $CsPbBr_3$ NCs substituted with 16%, 22%, and 45% Cl. For 16% Cl-substituted NCs, the Burstein–Moss effect is attenuated at high pumping intensities, and the HPB effect is slowed, accelerating HC cooling. For 45% Cl-substituted NCs, the further acceleration of HC cooling becomes negligible (Fig. 3(d)).[64] Interestingly, I-substituted $CsPbBr_3$ NCs may show slower cooling, likely due to the smaller high-frequency dielectric constant of iodide-based perovskites, weakening Fröhlich coupling and EP scattering.[65] Additionally, Ye *et al.*[46] found that in $CsPbBr_xI_{3-x}$ NCs, HC cooling becomes faster with increasing defect density, due to the reduction of HPB and Auger heating effects.

3.4. Impact of size

The size effect plays a significant role in modulating HC cooling behavior, primarily by altering energy levels via

quantum confinement, which in turn affects the HC cooling rate.[66,67] As reported by Li and coworkers,[19] the HC cooling rate of small $MAPbBr_3$ NCs is roughly half that of their bulk counterpart. This behavior can be attributed to the transformation from continuum to discrete energy levels as the size decreases. Although reducing the size enhances EP coupling,[68] quantum confinement remains dominant at the nanoscale. This causes excitons to release energy via Auger reheating,[69] which slows down HC cooling. Furthermore, the separation of energy levels limits phonon scattering channels, leading to a pronounced intrinsic phonon bottleneck effect during cooling, independent of carrier density.[70] Similarly, small $FASnI_3$ NCs exhibit HC cooling rates roughly half those of their larger counterparts, as shown in Fig. 4(a).[47]

It should be noted that the size effect on HC cooling is not completely linear, as Oriel *et al.*[66] recently reported. Although the cooling rate of $CsPbBr_3$ NCs under weakly confined conditions slows down as the size decreases, the HC rate accelerates when the size enters the strong confinement regime, as illustrated in Fig. 4(b). This observation aligns with previous studies by Kim *et al.*[59] and Cong *et al.*[39] They suggested that in strongly confined NCs, the HC cooling process is primarily governed by Auger recombination. This effect intensifies with decreasing size, enhancing Coulomb interactions and thereby suppressing the intrinsic phonon bottleneck effect, which would otherwise retard cooling.[71,72]

However, the influence of size on the HC cooling process remains controversial.[45] In 2017, Butkus *et al.*[62] studied $CsPbBr_3$ NCs with a size of 4.1 nm, smaller than the Bohr diameter of ~ 7 nm, and found that the HC time was nearly identical to that of NCs with sizes of 8.6 nm and 7.3 nm. They concluded that the intrinsic bottleneck effect originates from the material itself. Furthermore, enhanced quantum confinement does not cause significant changes in the electronic states or phonon distributions associated with HC cooling.[73] In 2019, Diroll *et al.*[74] observed a similar size-independent phenomenon in weakly confined $CsPbBr_3$ NCs (Fig. 4(c)). They suggested that the HC cooling process of these NCs is less affected by surface states. For strongly confined $CsPbBr_3$ NCs of varying sizes, Li *et al.*[75] reported that nonadiabatic coupling induced by surface ligands dominates, leading to similar HC cooling rates. In 2020, Boehme *et al.*[76] attributed the size-independent HC cooling time to the similar DOS in $CsPbBr_3$ NCs of different sizes, as shown in Fig. 4(d). Although size-dependent effects were observed in $CsPbBr_3$ NCs smaller than 0.8 nm, these were attributed to stoichiometric deviations arising from their ultra-small size, forming structures similar to Cs_4PbBr_6. Overall, this work suggests that size effects have minimal influence on HC cooling behavior in $CsPbBr_3$ NCs.

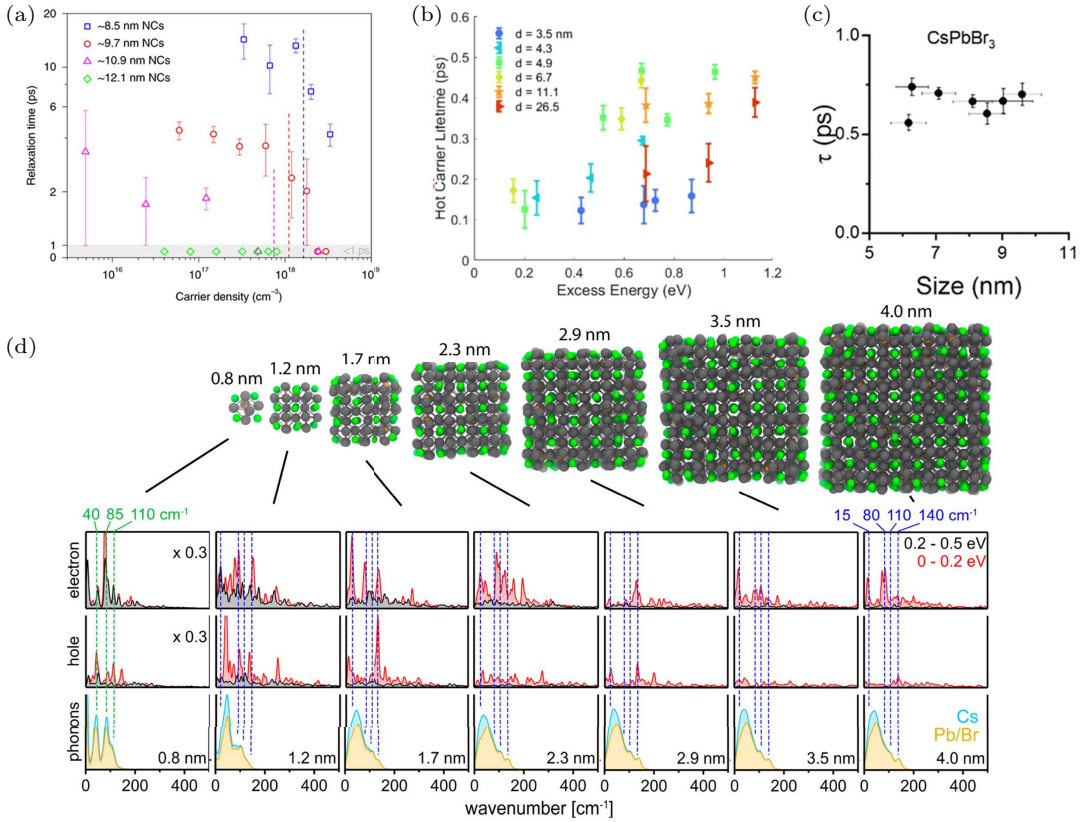


Fig. 4. (a) HC relaxation times of $FASnI_3$ NCs of different sizes at a given carrier density.[47] (b) HC lifetimes of $CsPbBr_3$ NCs with varying sizes under a given pump energy.[66] (c) HC lifetime constants of $CsPbBr_3$ NCs under pump excitation 1 eV above the bandgap.[74] (d) Electronic, hole, and phonon spectra of $CsPbBr_3$ NCs with different sizes. Phonon spectra are similar across all sizes, except for the smallest NC (0.8 nm).[76]

3.5. Impact of dimension

Quantum confinement effects significantly influence the HC cooling process. Compared to two-dimensional (2D) nanoplatelets (NPLs) and zero-dimensional (0D) NCs, one-dimensional (1D) $FAPbBr_3$ nanowires (NWs) exhibit intrinsically fast cooling, independent of carrier density.[77] In 2020, Shukla *et al.*[40] observed that 2D $CsPbBr_3$ nanosheets (NSs) exhibit stronger quantum effects than three-dimensional (3D) NCs, because strong quantum confinement causes electrons and holes to behave as individual particles rather than bound excitons,[77] enhancing their coupling, which leads to faster cooling than in 3D NCs.

Dimensionality affects not only quantum confinement but also interactions between carriers and phonons. Hintermayr *et al.*[12] found that 2D MAPI NPLs (layer $n = 1$) exhibit faster HC cooling than their quasi-2D (layer $n > 1$) counterparts. The expected HPB effect was absent despite reduced phonon states and density. This behavior arises from the larger surface-to-volume ratio at smaller layer numbers (n). It reduces the probability of in-plane thermal phonon reabsorption, allowing phonons to transfer energy to the surrounding environment, as shown in Fig. 5(a). In 2022, Villamil *et al.*[10,78,79] attributed the faster HC cooling rate with decreasing dimensionality to stronger quantum confinement, which enhances EP coupling and accelerates nonadiabatic recombination.[77,80] In 2023, Carwithen *et al.*[73] linked the suppression of the HPB effect in $CsPbBr_3$ NPLs to the larger exciton binding energy (Fig. 5(b)). In this regime, carrier–carrier scattering dominates the HC cooling mechanism, raising the critical phonon density required for the HPB effect. In 2024, Zhu *et al.*[81] reported that decreasing the number of layers (n) of $CsPbBr_3$ NPLs increases the defect density, increasing surface-defect-related nonadiabatic carrier processes, which accelerate cooling, as shown in Fig. 5(c).

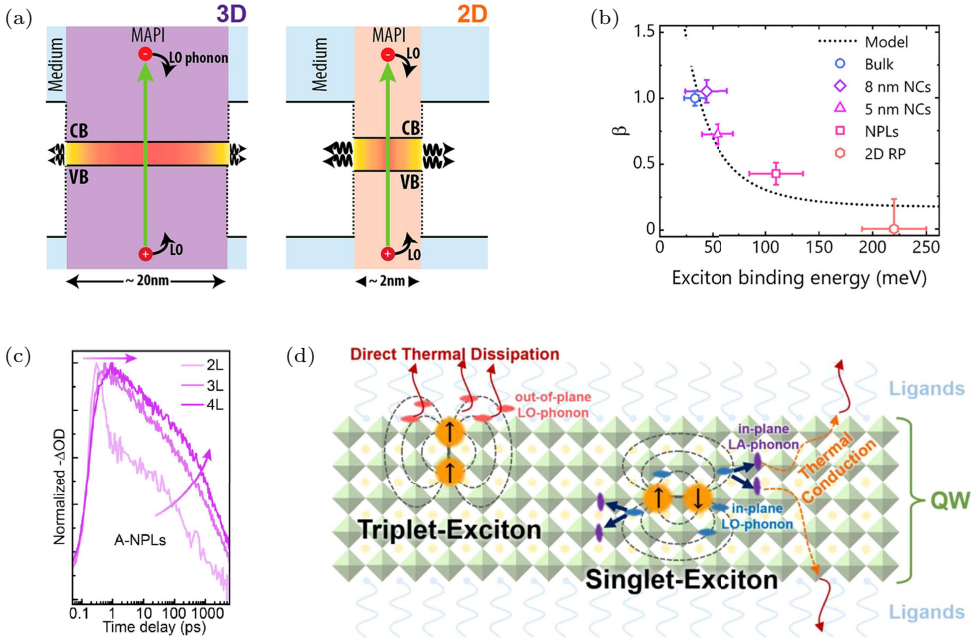


Fig. 5. (a) Schematic diagrams of HC cooling between quasi-2D/quasi-3D (layer $n > 1$) and 2D (layer $n = 1$) MAPI NPLs.[12] (b) Approximate inverse relationship between exciton binding energy and HPB effect density (β) in different $CsPbBr_3$ structures.[73] (c) Normalized ground-state bleaching dynamics of 2L, 3L, and 4L (layer $n = 2, 3, 4$) $CsPbBr_3$ NPLs.[81] (d) Schematic of the coupling mechanism among single excitons, triple excitons, and phonons in 2D NPL quantum wells.[83]

Moreover, the lower dielectric environment of the 2D NSs and NPLs reduces screening of the Fröhlich interaction[40,82] and facilitates rapid energy dissipation through direct contact with the surrounding environment.[10,12] In 2022, Sun *et al.*[83] observed that 2D few-monolayer $CsPbBr_3$ NPLs exhibit rapid HC cooling independent of carrier density, in contrast to the slower cooling in 0D and 3D $CsPbBr_3$ NCs due to the HPB effect. This suggests a unique heat dissipation mechanism in 2D quantum wells (QWs), which cannot be fully explained by conventional LO phonon scattering. To explain this, Sun *et al.*[83] proposed an out-of-plane triple exciton-phonon coupling mechanism, as shown in Fig. 5(d), where phonons rapidly dissipate into the out-of-plane environment following Fröhlich-like interactions with triple excitons, thereby preventing phonon accumulation and the HPB effect.

3.6. Impact of doping

Ion doping can create additional energy bands in semiconductor materials, which can affect the carrier relaxation process. Meng *et al.*[42] studied the HC cooling process in $CsPbI_3$ NCs doped with different concentrations of Mn ions. At an excitation energy of 3.1 eV, the HC cooling time exhibited a trend of first decreasing and then increasing as the doping concentration increased. At low doping concentration, the relaxation channel and enhanced EP coupling introduced by Mn doping dominate, thereby accelerating HC cooling. How-

ever, at high doping concentration, phonon bandgap widening induced by Mn doping dominates, slowing LO phonon decay and consequently reducing the HC cooling rate (Fig. 6(a)). Dai *et al.*[24] found that when a small amount of Sn ions was introduced into the Pb-iodide nanocrystalline systems, the carrier cooling rate of $MASn_xPb_{1-x}I_3$ became faster, which was attributed to an increase in defect density. However, when the Sn content is further increased, it leads to shielding of the Fröhlich interactions and increases the energy difference between LO and acoustic phonons. As a result, LO phonon decay through the Klemens channel is suppressed, and thermal conductivity decreases, affecting acoustic phonon transport. Collectively, these three mechanisms contribute to slower HC cooling in Sn–Pb alloyed NCs.

Defects may be passivated by doping, which can influence the HC cooling process. Dai *et al.*[24] reported that HC cooling of $CsSn_{0.4}Pb_{0.6}I_3$ NCs doped with Na ions exhibited slower HC cooling at both low and high pump intensities. This is because Na doping passivates sub-bandgap defect states and decouples HCs from these states, resulting in longer HC lifetimes, reduced energy loss rates, and a more pronounced HPB effect. Zhuang and coworkers observed that Sm^{3+}-doped $CsPbBrCl_2$ NCs (50.28 ps) exhibited a longer HC lifetime than $CsPbBrCl_2$ NCs (33.32 ps) (Fig. 6(b)). They concluded that Sm doping effectively passivates trap sites, thereby slowing carrier cooling.[84] In addition, Bose *et al.*[85] investigated the HC cooling process of Cu-doped $CsPbI_3$ NCs. They found that the Cu-doped NCs introduced shallow defect states of Cu 3d and Cu 4s in the conduction band, extending the Auger recombination time from 8.0 ± 0.4 ps to 12.0 ± 0.4 ps. This retained the phonon bottleneck effect and consequently prolonged the HC cooling time.

Niu *et al.*[30] investigated the HC cooling process of Ni-doped $CsPbI_3$ NCs. First-principles calculations confirm that Ni doping enhances electron–LO phonon coupling, generates additional energy states at the band edges, increases the effective carrier mass, and reduces the phonon bandgap, which contributes to the opening of the Klemens channel (Fig. 6(c)). The observed lifetimes of LO and acoustic phonons confirm that Ni doping facilitates the opening of Klemens channels, thus mitigating the HPB effect. Marjit *et al.*[86] reported that Bi-doped $CsPbBr_3$ NCs increased the density of states of low-energy optical phonons and the Born effective charge, both of which lead to higher EP scattering rates and the formation of localized energy bands within the conduction band (anti-defect states), accelerating HC cooling (Fig. 6(d)).

Notably, the type of defects has a significant impact on HC cooling times. Zhou *et al.*[87] demonstrated that, in contrast to vacancy point defects, interstitial point defects can reduce band degeneracy, weaken HC–phonon interactions, diminish nonadiabatic coupling, and ultimately slow down HC cooling by a factor of 1.5–2. Defect tolerance is crucial for achieving efficient lead halide perovskite materials. Ye *et al.*[46] investigated the influence of intentionally introduced traps on HC relaxation in $CsPbX_3$ (X = Br, I, or their mixtures) NCs . They demonstrated that perovskite NCs exhibit defect tolerance only in the presence of shallow traps. However, deeper traps accelerate HC cooling, thereby suppressing the hot phonon bottleneck and Auger reheating effects.

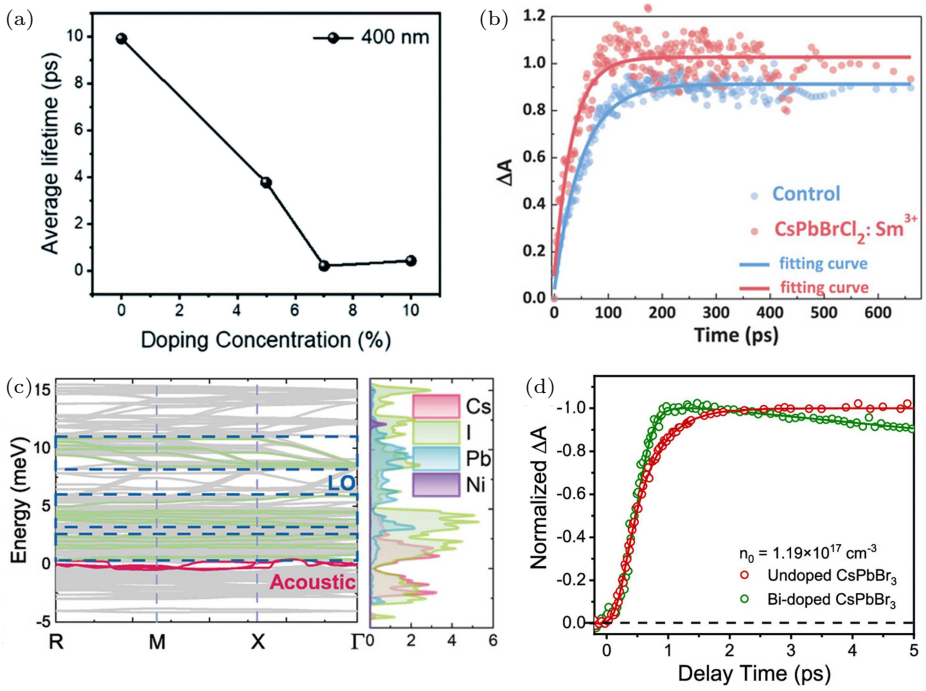


Fig. 6. (a) Average HC lifetime of $CsPbI_3$ NCs as a function of Mn-doping concentration.[42] (b) Normalized carrier decay fits of the control group (undoped) and Sm-doped $CsPbBrCl_2$ at 400 nm excitation.[84] (c) Phonon dispersion spectra of Ni-doped $CsPbI_3$ (left panel) and the projected density of states of different elements (right panel), with the red line indicating the acoustic phonon mode and the low-frequency LO phonon mode highlighted within the blue dashed box.[30] (d) Kinetics of bleaching signal formation of undoped and 5% Bi-doped $CsPbBr_3$ NCs at 3.1 eV excitation energy.[86]

Table 1. Comparison of HC cooling times of various perovskite NCs.

Influence factor	Samples	HC cooling time	Ref.
Component	$CsPbBr_3$	390 ± 20 fs ($\langle N_0\rangle\sim0.1$, 350 nm)	[27]
	$MAPbBr_3$	270 ± 20 fs ($\langle N_0\rangle\sim0.2$, 350 nm)	[27]
	$FAPbBr_3$	210 ± 20 fs ($\langle N_0\rangle\sim0.1$, 350 nm)	[27]
	$CsPbI_3$	0.38 ± 0.01 ps ($n_0\sim1.4\times10^{17}$–7.8×10^{17} cm^{-3}, 470 nm)	[53]
	$FAPbI_3$	0.29 ± 0.01 ps ($n_0\sim1.4\times10^{17}$–7.8×10^{17} cm^{-3}, 470 nm)	[53]
	$MAPbI_3$	0.25 ± 0.01 ps ($n_0\sim1.4\times10^{17}$–7.8×10^{17} cm^{-3}, 470 nm)	[53]
	$FA_{0.5}MA_{0.5}PbI_3$	7.9 ± 0.4 ps ($n_0\approx1\times10^{18}$ cm^{-3}, 470 nm)	[53]
	$FA_{0.5}Cs_{0.5}PbI_3$	8.4 ± 0.4 ps ($n_0\approx1\times10^{18}$ cm^{-3}, 470 nm)	[53]
	$MA_{0.5}Cs_{0.5}PbI_3$	6.8 ± 0.3 ps ($n_0\approx1\times10^{18}$ cm^{-3}, 470 nm)	[53]
	$CsPbBr_3$	570 fs (330 nm)	[95]
	$CsPb_{0.2}Cd_{0.8}Br_3$	233 ± 15 fs ($\langle N_0\rangle\sim0.6$, 330 nm)	[95]
	$CsPbBr_3$	396 fs ($\langle N_0\rangle\sim0.5$, 350 nm)	[60]
	$CsPb_{0.93}Cd_{0.07}Br_3$	350 fs ($\langle N_0\rangle\sim0.5$, 350 nm)	[60]
	$CsPb_{0.88}Cd_{0.12}Br_3$	314 fs ($\langle N_0\rangle\sim0.5$, 350 nm)	[60]
	$CsPbI_3$	804 fs ($\langle N_0\rangle\sim2.3$, 350 nm)	[61]
	$CsPb_{0.8}Zn_{0.2}I_3$	715 fs ($\langle N_0\rangle\sim2.7$, 350 nm)	[61]
	$CsPbBr_3$	0.60 ± 0.02 ps (400 nm)	[64]
	$CsPb(Br_{0.84}Cl_{0.16})_3$	0.41 ± 0.01 ps (400 nm)	[64]
	$CsPb(Br_{0.78}Cl_{0.22})_3$	0.41 ± 0.01 ps (400 nm)	[64]
	$CsPb(Br_{0.55}Cl_{0.45})_3$	0.41 ± 0.01 ps (400 nm)	[64]
	$CsPbBr_3$	3.8 ± 0.3 ps ($n_0\sim12.5\times10^{17}$ cm^{-3}, 400 nm)	[46]
	$CsPbBr_xI_{3-x}$	7.1 ± 0.1 ps ($n_0\sim58.0\times10^{17}$ cm^{-3}, 400 nm)	[46]
Size	$MAPbBr_3$ (4.9 nm)	~0.7 ps ($n_0=15\times10^{17}$ cm^{-3}, 800 nm)	[19]
	$MAPbBr_3$ (8.9 nm)	~0.6 ps ($n_0=2.6\times10^{17}$ cm^{-3}, 800 nm)	[19]
	$MAPbBr_3$ (11.6 nm)	~0.5 ps ($n_0=1.4\times10^{17}$ cm^{-3}, 800 nm)	[19]
	$FASnI_3$ (10.9 nm)	3.35 ± 2.36 ps (400 nm)	[47]
	$FASnI_3$ (9.7 nm)	4.42 ± 0.51 ps (400 nm)	[47]
	$FASnI_3$ (8.5 nm)	14.3 ± 3.2 ps (400 nm)	[47]
	$MAPbBr_3$ (1.9 nm)	0.7 ps ($\langle N_0\rangle\approx2.5$)	[59]
	$MAPbBr_3$ (4.9 nm)	1.2 ps ($\langle N_0\rangle\approx2.5$)	[59]
	$MAPbBr_3$ (9.6 nm)	4.4 ps ($\langle N_0\rangle\approx2.5$)	[59]
	$CsPbBr_3$ (8.6 nm)	319 ± 54 fs (400 nm)	[62]
	$CsPbBr_3$ (7.3 nm)	325 ± 31 fs (400 nm)	[62]
	$CsPbBr_3$ (4.1 nm)	363 ± 20 fs (400 nm)	[62]
Dimension	0D $MAPbBr_3$	0.28 ps ($n_0\sim2\times10^{18}$ cm^{-3}, 388 nm)	[77]
	1D $MAPbBr_3$	0.23 ps ($n_0\sim2\times10^{18}$ cm^{-3}, 388 nm)	[77]
	2D $MAPbBr_3$	0.34 ps ($n_0\sim2\times10^{18}$ cm^{-3}, 388 nm)	[77]
	2D $CsPbBr_3$ 3L-NPLs	82 fs (375 nm)	[81]
	2D $CsPbBr_3$ 4L-NPLs	119 fs (384 nm)	[81]
	2D $CsPbBr_3$ 2L-NPLs	140 ± 10 fs ($\langle N_0\rangle\sim0.15$, 400 nm)	[82]
	2D $CsPbBr_3$ 3L-NPLs	167 ± 15 fs ($\langle N_0\rangle\sim0.15$, 400 nm)	[82]
	2D $CsPbBr_3$ 4L-NPLs	210 ± 20 fs ($\langle N_0\rangle\sim0.15$, 400 nm)	[82]
	2D $CsPbBr_3$ 5L-NPLs	~0.3 ps ($\langle N_0\rangle=8.4$, 400 nm)	[83]
Doping	$CsPbI_3$	710 fs ($\langle N_0\rangle\sim0.1$, 340 nm)	[30]
	Ni:$CsPbI_3$	620 fs ($\langle N_0\rangle\sim0.1$, 340 nm)	[30]
	$CsPbBrCl_2$	33.32 ps (400 nm)	[84]
	$CsPbBrCl_2$:Sm^{3+}	50.28 ps (400 nm)	[84]
	$CsPbI_3$	0.39 ± 0.04 ps (400 nm)	[85]
	Cu:$CsPbI_3$	0.47 ± 0.04 ps (400 nm)	[85]
	$CsPbBr_3$	560 ± 10 fs (400 nm)	[86]
	5% Bi-doped $CsPbBr_3$	400 ± 15 fs (400 nm)	[86]
	10% Bi-doped $CsPbBr_3$	300 ± 14 fs (400 nm)	[86]
Epitaxial shell	$CsPbBr_3$	560 ± 8 fs ($\langle N_0\rangle\sim1.5$, 400 nm)	[9]
	$CsPbBr_3$/Cs_4PbBr_6	265 ± 5 fs ($\langle N_0\rangle\sim1.5$, 400 nm)	[9]
	$MAPbBr_3$	194 fs ($\langle N_0\rangle\sim0.4$, 350 nm)	[93]
	$MAPbBr_3$/$MA_{1-x}Cs_xPbBr_3$	194 fs ($\langle N_0\rangle\sim0.4$, 350 nm)	[93]
	$CsPbBr_3$@ZnS	220 fs ($\langle N_0\rangle\sim0.4$, 400 nm)	[94]
	$CsPbBr_3$	490 fs ($\langle N_0\rangle\sim0.4$, 400 nm)	[94]

3.7. Impact of epitaxial shell

Perovskite NCs are susceptible to thermal instability and environmental degradation, which compromises their performance.[88] To address this, epitaxial growth of a shell material on the NC core can provide a physical barrier, passivate surface trap states, and enhance the fluorescence quantum yield.[89,90]

Kaur *et al.*[91,92] grew Cs_4PbBr_6 shell layers with a larger bandgap on $CsPbBr_3$ NCs. They observed that strong Fröhlich interactions in $CsPbBr_3$@Cs_4PbBr_6 lead to large polaron formation, which slows HC cooling. At higher bandgap excitation (300 nm), carriers are generated in both the core and shell, enhancing carrier redistribution between the core and shell, and further slowing cooling (Fig. 7(a)).

Our group found that the HC cooling times of $MAPbBr_3$ and $MAPbBr_3$@$MA_{1-x}Cs_xPbBr_3$ NCs are roughly comparable at low excitation intensities ($\sim$ 194 fs). At high excitation intensities, the cooling time of the core/shell NCs ($\sim$420 fs) is significantly longer than that of bare cores (252 fs). Temperature-dependent luminescence spectra indicate that the slower HC cooling in the core/shell NCs is likely due to weaker EP coupling.[93]

Nie *et al.*[9] reported epitaxial growth of Cs_4PbBr_6 on $CsPbBr_3$ NCs via interface engineering. They found that the HC cooling time was significantly shortened from 560 ± 8 fs to 265 ± 5 fs at 400 nm pump excitation. Computational analysis revealed that interfacial coupling between the LO phonons of Cs_4PbBr_6 and electrons in $CsPbBr_3$ NCs facilitates rapid HC cooling. The low energy and large number of LO phonons in Cs_4PbBr_6 activate an effective Klemens channel.

Ren *et al.*[94] found that in $CsPbBr_3$@ZnS NCs, hot holes from the $CsPbBr_3$ core are transferred to the ZnS shell. The excess energy of these hot holes is dissipated via ZnS phonons, reducing hot-phonon accumulation in $CsPbBr_3$ NCs and accelerating HC cooling, while diminishing sensitivity to excitation intensity (Figs. 7(b) and 7(c)).

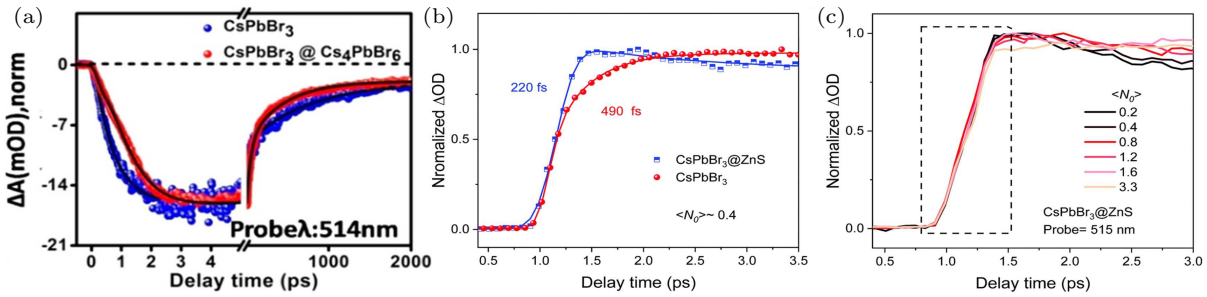


Fig. 7. (a) Comparative kinetics of $CsPbBr_3$@Cs_4PbBr_6 core/shell NCs monitored via band-edge bleaching.[91] (b) Band-edge photobleaching rise times of $CsPbBr_3$ and $CsPbBr_3$@ZnS NCs under 400 nm excitation.[94] (c) Normalized band-edge bleaching dynamics of $CsPbBr_3$@ZnS NCs at different excitation intensities.[94]

To facilitate readers' understanding of the factors influencing HC cooling dynamics in perovskite NCs, we provide a comparative analysis of HC cooling times across different materials reported in the literature, as summarized in Table 1. Here, $\langle N_0 \rangle$ denotes the average number of excitons generated per NC, and n_0 represents the carrier density.

4. Conclusion and perspectives

Based on the above discussions, it is evident that HC cooling is a complex process influenced by multiple factors, with some effects being controversial or occasionally contradictory. Nevertheless, certain aspects have reached a consensus in the research community.

(i) The excitation energy directly impacts the HC cooling process. Generally, increasing the excitation energy prolongs HC cooling time. However, when the excitation energy exceeds the multiple exciton generation threshold, the HC cooling process may be accelerated.

(ii) Two-dimensional perovskite materials, such as perovskite NSs and NPLs, typically exhibit out-of-plane scattering channels, which contribute to the suppression of HPB effects even at high carrier densities. Additionally, 2D perovskite NSs and NPLs possess higher exciton binding energies than 3D NCs, enhancing Coulombic interactions, which often results in faster HC cooling rates compared to 3D NCs under the same conditions.

(iii) Doping with certain metal ions (e.g., Sm^{3+}, Cu^{2+}) may passivate defects in perovskite NCs, thereby slowing HC cooling. Conversely, introduction of metal ions such as Ni^{2+} and Bi^{3+} can enhance EP coupling, accelerating the HC cooling process.

(iv) Core–shell structures can significantly influence HC cooling. On one hand, they facilitate the transfer of HCs from the core to the shell, reducing the number of hot phonons in the core and accelerating HC cooling. On the other hand, they may also induce the formation of large polarons, which can slow down HC cooling.

Given the unresolved challenges in HC cooling dynamics within perovskite NCs, future investigations should prioritize the following directions:

(i) Defect engineering and trap-state modulation. The impact of defects on HC cooling is complex. Systematic studies are needed to elucidate how different defect types (e.g., vacancies, interstitials, dopants) influence HC relaxation path-

ways and to establish quantitative correlations between defect energy levels and cooling rates.

(ii) Multiscale modeling. Existing theoretical models require closer integration with experimental data. Combining nonadiabatic molecular dynamics simulations with first-principles calculations could reveal atomic-level mechanisms of HC cooling influenced by defects, interfaces, and lattice vibrations.

(iii) Interplay of multiple factors. While individual factors affecting HC cooling have been well investigated, few studies have systematically explored their combined effects. Given the prevalence of multifactorial influences in practical applications, it is imperative to elucidate how multiple factors collectively modulate HC cooling dynamics.

(iv) Interdisciplinary collaboration. Through interdisciplinary efforts spanning materials design, theoretical modeling, and advanced characterization, researchers can overcome current bottlenecks in HC energy loss and propel perovskite optoelectronic devices beyond conventional efficiency limits.

Acknowledgments

This work was supported by the National Natural Science Foundation of China (Grant Nos. 62475169 and 62174079), the Guangdong Basic and Applied Basic Research Foundation (Grant No. 2025A1515011195), the Guangdong Provincial Quantum Science Strategic Initiative (Grant No. GDZX2404006), the Shenzhen Science and Technology Program (Grant Nos. JCYJ20240813143212016 and JCYJ20231122200233001), and the Post-doctoral Later-stage Foundation Project of Shenzhen Polytechnic University (Grant No. 6024271003K).

References

[1] Kim Y H, Park J, Kim S, Kim J S, Xu H, Jeong S H, Hu B and Lee T W 2022 *Nat. Nanotechnol.* **17** 590
[2] Ko P K, Chen D, Li C H A, Chan C C S, Sergeev A, Ding P, Lam D, Ouyang B, Guo L, Wong K S and Halpert J E 2024 *Chem. Mater.* **36** 3735
[3] Liao Q, Jin X and Fu H 2019 *Adv. Opt. Mater.* **7** 1900099
[4] Liu A, Guan G, Chai X, Feng N, Lu M, Bai X and Zhang Y 2022 *Laser Photonics Rev.* **16** 2200189
[5] Zhu H, Fu Y, Meng F, Wu X, Gong Z, Ding Q, Gustafsson M V, Trinh M T, Jin S and Zhu X Y 2015 *Nat. Mater.* **14** 636
[6] Zhang X, Xiao S, Wang X, He T and Chen R 2023 *Chin. Phys. B* **32** 064212
[7] Polavarapu L, Nickel B, Feldmann J and Urban A S 2017 *Adv. Energy Mater.* **7** 1700267
[8] Huang H, Bodnarchuk M I, Kershaw S V, Kovalenko M V and Rogach A L 2017 *ACS Energy Lett.* **2** 2071
[9] Nie Z, Gao X, Ren Y, Xia S, Wang Y, Shi Y, Zhao J and Wang Y 2020 *Nano Lett.* **20** 4610
[10] Villamil Franco C, Trippé-Allard G, Mahler B, Cornaggia C, Lauret J S, Gustavsson T and Cassette E 2022 *J. Phys. Chem. Lett.* **13** 393
[11] Ahmed I, Shi L, Pasanen H, Vivo P, Maity P, Hatamvand M and Zhan Y 2021 *Light-Sci. Appl.* **10** 174
[12] Hintermayr V A, Polavarapu L, Urban A S and Feldmann J 2018 *ACS Nano* **12** 10151
[13] Brinkmann K O, Wang P, Lang F, Li W, Guo X, Zimmermann F, Olthof S, Neher D, Hou Y, Stolterfoht M, Wang T, Djurišić A B and Riedl T 2024 *Nat. Rev. Mater.* **9** 202
[14] Wetzelaer G J A H, Scheepers M, Sempere A M, Momblona C, Avila J and Bolink H J 2015 *Adv. Mater.* **27** 1837
[15] Chan C C S, Fan K, Wang H, Huang Z, Novko D, Yan K, Xu J, Choy W C H, Lončarić I and Wong K S 2021 *Adv. Energy Mater.* **11** 2003071
[16] Wang H I, Infante I, Brinck S t, Cánovas E and Bonn M 2018 *Nano Lett.* **18** 5111
[17] Dursun I, Maity P, Yin J, Turedi B, Zhumekenov A A, Lee K J, Mohammed O F and Bakr O M 2019 *Adv. Energy Mater.* **9** 1900084
[18] Zhou Z, Wu Y, He J, Frauenheim T and Prezhdo O V 2024 *J. Am. Chem. Soc.* **146** 29905
[19] Li M, Bhaumik S, Goh T W, Kumar M S, Yantara N, Grätzel M, Mhaisalkar S, Mathews N and Sum T C 2017 *Nat. Commun.* **8** 14350
[20] Chen K, Barker A J, Morgan F L C, Halpert J E and Hodgkiss J M 2015 *Phys. Chem. Lett.* **6** 153
[21] Yang Y, Ostrowski D P, France R M, Zhu K, van de Lagemaat J, Luther J M and Beard M C 2016 *Nat. Photonics* **10** 53
[22] Shi H, Zhang X, Li R and Zhang X 2023 *Nanomaterials* **13** 3134
[23] Mondal N, Carwithen B P and Bakulin A A 2023 *Light-Sci. Appl.* **12** 1
[24] Dai L, Ye J and Greenham N C 2023 *Light-Sci. Appl.* **12** 208
[25] Tekelenburg E K, Camargo F V A, Filippetti A, Mattoni A, van de Ven L J M, Pitaro M, Cerullo G and Loi M A 2025 *Adv. Mater.* **37** 2411892
[26] Zhu L, Zhao R, Zhuang R, Wu T, Xie L and Hua Y 2022 *EcoMat* **5** e12313
[27] Chen J, Messing M E, Zheng K and Pullerits T 2019 *J. Am. Chem. Soc.* **141** 3532
[28] Paul K K, Kim J H and Lee Y H 2021 *Nat. Rev. Phys.* **3** 178
[29] Marjit K, Das A, Ghosh D and Patra A 2024 *ChemNanoMat* **10** e202300629
[30] Niu W, Chen R, Pang T, Zheng Y, Wu T, Zhang R and Chen D 2024 *Adv. Opt. Mater.* **12** 2400307
[31] Forde A, Inerbaev T, Hobbie E K and Kilin D S 2019 *J. Am. Chem. Soc.* **141** 4388
[32] Kaur G and Ghosh H N 2020 *Phys. Chem. Lett.* **11** 8765
[33] Li M, Fu J, Xu Q and Sum T C 2019 *Adv. Mater.* **31** 1802486
[34] Fu J, Xu Q, Han G, Wu B, Huan C H A, Leek M L and Sum T C 2017 *Nat. Commun.* **8** 1300
[35] Nie Z, Huang Z, Zhang M, Wu B, Wu H, Shi Y, Wu K and Wang Y 2022 *ACS Photonics* **9** 3457
[36] Wei Q, Yin J, Bakr O M, Wang Z, Wang C, Mohammed O F, Li M and Xing G 2021 *Angew. Chem. Int. Ed.* **60** 10957
[37] Maity P, Merdad N A, Yin J, Lee K J, Sinatra L, Bakr O M and Mohammed O F 2021 *ACS Energy Lett.* **6** 2602
[38] Faber T, Filipovic L and Koster L J A 2024 *J. Phys. Chem. Lett.* **15** 12601
[39] Cong M, Yang B, Chen J, Hong F, Yang S, Deng W and Han K 2020 *J. Phys. Chem. Lett.* **11** 1921
[40] Shukla A, Kaur G, Babu K J, Ghorai N, Goswami T, Kaur A and Ghosh H N 2020 *J. Phys. Chem. Lett.* **11** 6344
[41] Li M, Begum R, Fu J, Xu Q, Koh T M, Veldhuis S A, Grätzel M, Mathews N, Mhaisalkar S and Sum T C 2018 *Nat. Commun.* **9** 4197
[42] Meng J, Lan Z, Lin W, Liang M, Zou X, Zhao Q, Geng H, Castelli I E, Canton S E, Pullerits T and Zheng K 2022 *Chem. Sci.* **13** 1734
[43] Zhang Y, Lou X, Chi X, Wang Q, Sui N, Kang Z, Zhou Q, Zhang H, Li L and Wang Y 2021 *J. Lumines.* **239** 118332
[44] Papagiorgis P, Protesescu L, Kovalenko M V, Othonos A and Itskos G 2017 *J. Phys. Chem. C* **121** 12434
[45] Hopper T R, Gorodetsky A, Jeong A, Krieg F, Bodnarchuk M I, Maimaris M, Chaplain M, Macdonald T J, Huang X, Lovrincic R, Kovalenko M V and Bakulin A A 2020 *Nano Lett.* **20** 2271
[46] Ye J, Mondal N, Carwithen B P, Zhang Y, Dai L, Fan X B, Mao J, Cui Z, Ghosh P, Otero-Martinez C, van Turnhout L, Huang Y T, Yu Z, Chen Z, Greenham N C, Stranks S D, Polavarapu L, Bakulin A, Rao A and Hoye R L Z 2024 *Nat. Commun.* **15** 8120
[47] Dai L, Deng Z, Auras F, Goodwin H, Zhang Z, Walmsley J C, Bristowe P D, Deschler F and Greenham N C 2021 *Nat. Photonics* **15** 696
[48] Yang J, Wen X, Xia H, Sheng R, Ma Q, Kim J, Tapping P, Harada T, Kee T W, Huang F, Cheng Y B, Green M, Ho-Baillie A, Huang S, Shrestha S, Patterson R and Conibeer G 2017 *Nat. Commun.* **8** 14120
[49] Marjit K, Francis A G, Pati S K and Patra A 2023 *J. Phys. Chem. Lett.* **14** 10900
[50] Shrivastava M, Bodnarchuk M I, Hazarika A, Luther J M, Beard M C, Kovalenko M V and Adarsh K V 2020 *Adv. Opt. Mater.* **8** 2001016

[51] Zhu H, Miyata K, Fu Y, Wang J, Joshi P P, Niesner D, Williams K W, Jin S and Zhu X Y 2016 *Science* **353** 1409

[52] Zhu X Y and Podzorov V 2015 *Phys. Chem. Lett.* **6** 4758

[53] Li H, Wang Q, Oteki Y, Ding C, Liu D, Guo Y, Li Y, Wei Y, Wang D, Yang Y, Masuda T, Chen M, Zhang Z, Sogabe T, Hayase S, Okada Y, Iikubo S and Shen Q 2023 *Adv. Mater.* **35** 2301834

[54] Ji X, Lu R and Yu A 2023 *J. Phys. Chem. C* **127** 19579

[55] Huang Y, Guo C, Gao L, Du W, Zheng H, Wu D, Zhao Z, Zhang C W, Wang Q, Liu X F, Yan Q and Jiang Y 2024 *Chin. Phys. B* **33** 107304

[56] Li Y, Ding T, Luo X, Tian Y, Lu X and Wu K 2020 *Chem. Mater.* **32** 549

[57] Hopper T R, Gorodetsky A, Frost J M, Müller C, Lovrincic R and Bakulin A A 2018 *ACS Energy Lett.* **3** 2199

[58] Qin Y, Li J, Hu J and He T 2024 *J. Phys. Chem. C* **128** 1202

[59] Kim T, Jung S I, Ham S, Chung H and Kim D 2019 *Small* **15** 1900355

[60] Li J, Guo Z, Xiao S, Tu Y, He T and Zhang W 2022 *Inorg. Chem.* **61** 4735

[61] Zhao F, Li J, Yu J, Guo Z, Xiao S, Gao Y, Pan R, He T and Chen R 2020 *J. Phys. Chem. C* **124** 27169

[62] Butkus J, Vashishtha P, Chen K, Gallaher J K, Prasad S K K, Metin D Z, Laufersky G, Gaston N, Halpert J E and Hodgkiss J M 2017 *Chem. Mater.* **29** 3644

[63] Kawai H, Giorgi G, Marini A and Yamashita K 2015 *Nano Lett.* **15** 3103

[64] Soetan N, Puretzky A, Reid K, Boulesbaa A, Zarick H F, Hunt A, Rose O, Rosenthal S, Geohegan D B and Bardhan R 2018 *ACS Photonics* **5** 3575

[65] Wright A D, Verdi C, Milot R L, Eperon G E, Pérez-Osorio M A, Snaith H J, Giustino F, Johnston M B and Herz L M 2016 *Nat. Commun.* **7** 11755

[66] Oriel E H, Dirin D N, Shcherbak K, Bodnarchuk M I, Kovalenko M V, Chen L X and Schaller R D 2024 *J. Phys. Chem. Lett.* **15** 6062

[67] Lim J W M, Guo Y, Feng M, Cai R and Sum T C 2024 *J. Am. Chem. Soc.* **146** 437

[68] Cho K, Tahara H, Yamada T, Suzuura H, Tadano T, Sato R, Saruyama M, Hirori H, Teranishi T and Kanemitsu Y 2022 *Nano Lett.* **22** 7674

[69] Klimov V I, Mikhailovsky A A, McBranch D W, Leatherdale C A and Bawendi M G 2000 *Science* **287** 1011

[70] Yu B, Chen L, Qu Z, Zhang C, Qin Z, Wang X and Xiao M 2021 *J. Phys. Chem. Lett.* **12** 238

[71] Strandell D P, Zenatti D, Nagpal P, Ghosh A, Dirin D N, Kovalenko M V and Kambhampati P 2024 *ACS Nano* **18** 1054

[72] Baker H, Perez C M, Sonnichsen C, Strandell D, Prezhdo O V and Kambhampati P 2023 *ACS Nano* **17** 3913

[73] Carwithen B P, Hopper T R, Ge Z, Mondal N, Wang T, Mazlumian R, Zheng X, Krieg F, Montanarella F, Nedelcu G, Kroll M, Siguan M A, Frost J M, Leo K, Vaynzof Y, Bodnarchuk M I, Kovalenko M V and Bakulin A A 2023 *ACS Nano* **17** 6638

[74] Diroll B T and Schaller R D 2019 *Adv. Funct. Mater.* **29** 1901725

[75] Li Y, Lai R, Luo X, Liu X, Ding T, Lu X and Wu K 2019 *Chem. Sci.* **10** 5983

[76] Boehme S C, Brinck S t, Maes J, Yazdani N, Zapata F, Chen K, Wood V, Hodgkiss J M, Hens Z, Geiregat P and Infante I 2020 *Nano Lett.* **20** 1819

[77] Telfah H, Jamhawi A, Teunis M B, Sardar R and Liu J 2017 *J. Phys. Chem. C* **121** 28556

[78] Tao W, Zhang Y and Zhu H 2022 *Accounts Chem. Res.* **55** 345

[79] El-Ballouli A a O, Bakr O M and Mohammed O F 2020 *J. Phys. Chem. Lett.* **11** 5705

[80] Zhang X, Gao X, Pang G, He T, Xing G and Chen R 2019 *J. Phys. Chem. C* **123** 28893

[81] Zhu Y, Luo S, Zhang Y, Liu Y, He Y, Li T, Chi Z and Guo L 2024 *Nanoscale* **17** 584

[82] Marjit K, Ghosh G, Ghosh S, Sain S, Ghosh A and Patra A 2021 *J. Phys. Chem. C* **125** 12214

[83] Sun Q, Gong J, Yan X, Wu Y, Cui R, Tian W, Jin S and Wang Y 2022 *Nano Lett.* **22** 2995

[84] Zhuang X, Sun R, Zhou D, Liu S, Wu Y, Shi Z, Zhang Y, Liu B, Chen C, Liu D and Song H 2022 *Adv. Funct. Mater.* **32** 2110346

[85] Bose S, Sharma A, Mahato S, Maurya N C, Roy B, Srivastava S K, Adarsh K V and Ray S K 2024 *Appl. Phys. Lett.* **124** 011901

[86] Marjit K, Ghosh G, Biswas R K, Ghosh S, Pati S K and Patra A 2022 *J. Phys. Chem. Lett.* **13** 5431

[87] Zhou Z, He J, Frauenheim T, Prezhdo O V and Wang J 2022 *J. Am. Chem. Soc.* **144** 18126

[88] Zhang C, Chen J, Kong L, Wang L, Wang S, Chen W, Mao R, Turyanska L, Jia G and Yang X 2021 *Adv. Funct. Mater.* **31** 2100438

[89] Ahmed G H, Yin J, Bakr O M and Mohammed O F 2021 *ACS Energy Lett.* **6** 1340

[90] Reiss P, Protière M and Li L 2009 *Small* **5** 154

[91] Kaur G, Justice Babu K, Ghorai N, Goswami T, Maiti S and Ghosh H N 2019 *Phys. Chem. Lett.* **10** 5302

[92] Kaur G, Shukla A, Babu K J and Ghosh H N 2022 *Chem. Rec.* **22** e202200106

[93] Li J, Guo Z, Xiao S, Tu Y, He T and Zhang W 2022 *Inorg. Chem. Front.* **9** 2980

[94] Ren Y, Nie Z, Deng F, Wang Z, Xia S and Wang Y 2021 *Nanoscale* **13** 292

[95] Gao Y, Cui Y, Li J, Xu Y, Hu J and He T 2022 *J. Phys. Chem. C* **126** 6694